*Computers and Geotechnics* **5** (1988) 269–284

# COMPARATIVE ANALYSIS OF SOME GEOMECHANICS PROBLEMS USING FINITE AND INFINITE ELEMENT METHODS

Gopal R. Karpurapu and R.J. Bathurst

Department of Civil Engineering
Royal Military College of Canada
Kingston, Ontario, Canada K7K 5L0

## ABSTRACT

Four classical geomechanics problems involving semi-infinite linear elastic media have been solved numerically using recently developed mapped infinite elements coupled to finite elements. The effect of the remoteness of the truncated boundary and the location of infinite element coupling on solution accuracy has been studied. The results of conventional analyses using finite elements over a relatively large but restricted region are compared to the coupled analyses. Comparison of the results shows that for the same number of degrees of freedom the performance of the coupled solutions is superior to the conventional approach with respect to accuracy of solution and computational efficiency. Finally, some general guidelines are proposed for the efficient numerical solution of these types of problems using the coupled finite/infinite element approach.

## INTRODUCTION

In the modelling of many geomechanics problems involving soil-structure interaction, the soil is represented as a region of semi-infinite extent. When these problems are formulated through analytical schemes, the modelling of the semi-infinite nature of the soil region is preserved explicitly as part of the solution procedure. When considering the numerical modelling of such problems using finite element techniques, the traditional approach to achieve the effect of unboundness is to incorporate a large number of elements extending significant distances beyond the range of the loaded region. However, the use of such large finite element discretizations, may result in a large amount of computational effort. Also, the location of the truncated boundary is indeterminate, and an arbitrary location may lead to erroneous results. In practice, a compromise is often made between solution accuracy and computational effort. Nevertheless, the level of discretization and



*Computers and Geotechnics* 0266-352X/88/$03·50 

the location of the truncated boundary selected is often based on trial and error before an acceptable degree of accuracy is achieved.

Many techniques have been proposed in the past for the numerical modelling of unbounded media [1-7]. They range from semi-analytical methods (in which infinite elements are constructed on the basis of far field solutions) to exponential decay methods which ensure the decay of variables at large distances. Exponential decay methods have the disadvantage that their implementation is problem dependent and they require specialized numerical integration [1].

Recently some of the above problems have been overcome by the introduction of mapped infinite elements. There are basically two methods of formulating these elements. One method is the direct approach, or the displacement *descent* method, in which the natural coordinate domain is extended to infinity in the required direction while keeping the standard mapping functions well-defined. The unknown variables are expressed in terms of descent shape functions which decay asymptotically to zero towards infinity [1,2]. The second approach is the inverse method, or the coordinate *ascent* method, in which the domain of the natural plane (e.g. $-1 \leq \xi \leq +1$) is maintained as usual [3,4,5,6,7]. Ascent mapping functions are employed for geometries that are singular at an extreme of the natural plane (e.g. $\xi = +1$) causing the physical coordinate to exhibit singular behaviour when the natural coordinate approaches that extreme. The physical coordinate value at the extreme of natural plane (e.g. $\xi = +1$) approaches infinity and hence the element represents an unbounded medium. Conventional shape functions are employed for interpolating nodal variables. Of these two approaches, the latter is preferred as it uses the conventional Gauss-Legendre numerical integration for element formulations. This feature facilitates their implementation in general purpose finite element programs without major modifications.

## MAPPED INFINITE ELEMENT

The concept of the coordinate ascent mapped infinite element has been explained in detail in other publications [e.g. 3,4,5,6,7]. Hence the discussion in this section is restricted to the basic derivation of mapping and shape functions of this element.

Mapped infinite elements can be constructed to represent various orders of decay rate for the field variables. Of all the decay rates reported in the literature, the $1/r$ type seems to yield the most accurate results [e.g. 5,6,7] and has been adopted in the current investigation. Figure 1 shows a five-noded infinite element which represents an infinite medium in the local coordinate direction $\xi$. Mapping functions for the element nodes can be constructed separately in the two local directions $\xi$ and $\eta$ and the global functions

obtained as their product according to:

$$M_i = M_i(\xi)M_i(\eta) \tag{1}$$

The mapping function in local direction $\xi$ is constructed with the singularity at the $\xi = +1$ face (i.e. infinite distance). For example, local direction mapping functions for nodes 1 and 5 can be obtained as follows:

$$M_1(\xi) = \frac{-2\xi}{(1-\xi)} \tag{2}$$

$$M_1(\eta) = \frac{\eta(1+\eta)}{2} \tag{3}$$

$$M_5(\xi) = \frac{(1+\xi)}{(1-\xi)} \tag{4}$$

$$M_5(\eta) = \frac{(1+\eta)}{2} \tag{5}$$

Interpolation for the field variables of infinite elements is normally carried out in terms of nodal variables at the finitely located nodes assuming that the variables vanish to zero at infinite distance. By invoking this assumption, the infinite element shown in Figure 1 can be considered as an analogue of an 8-noded quadrilateral element whose field variables on the three nodes at the $\xi = +1$ face are zero. The shape functions for the infinite element nodes are then obtained directly from the corresponding nodes of an 8-noded isoparametric quadrilateral element. Table 1 gives a complete listing of mapping and shape functions.

Both functions satisfy completeness and monotonic convergence requirements and hence the mapping is independent of the choice of coordinate system and the interpolation yields unique values. It was found that a lower order of integration for the infinite elements than that of finite elements in assemblage yields better results [7]. Hence an integration order of $2 \times 2$ and $3 \times 3$ has been used for infinite and finite elements respectively to formulate various element matrices in the numerical analyses to follow.

## NUMERICAL ANALYSIS AND RESULTS

Four classical geomechanics problems are selected and their numerical solutions determined using *conventional* finite element methods and *coupled* methods that employ a region of finite elements surrounded by a semi-infinite domain modelled by infinite elements.

In the conventional analyses the distance to the truncated boundary is varied whereas in the coupled analyses the distance to the coupling location is varied. In each analysis a *remoteness factor* $\beta$, has been defined in terms of distance to the boundary and a characteristic length of the structure under consideration. In both methods of analysis, the number of elements and consequently the number of nodal points has been increased for higher

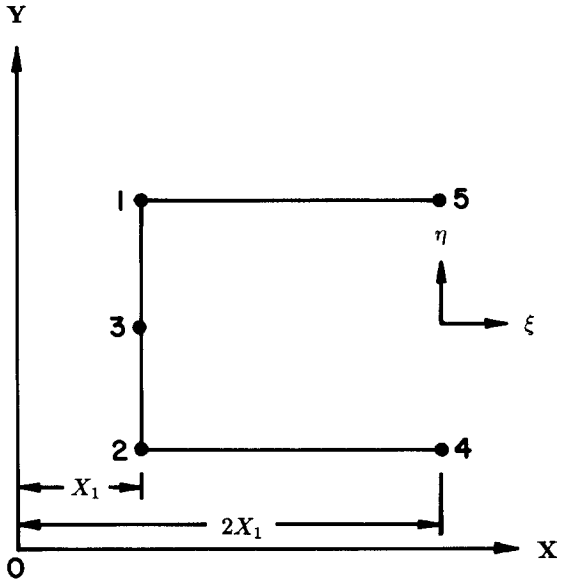


FIGURE 1. Two-dimensional mapped infinite element

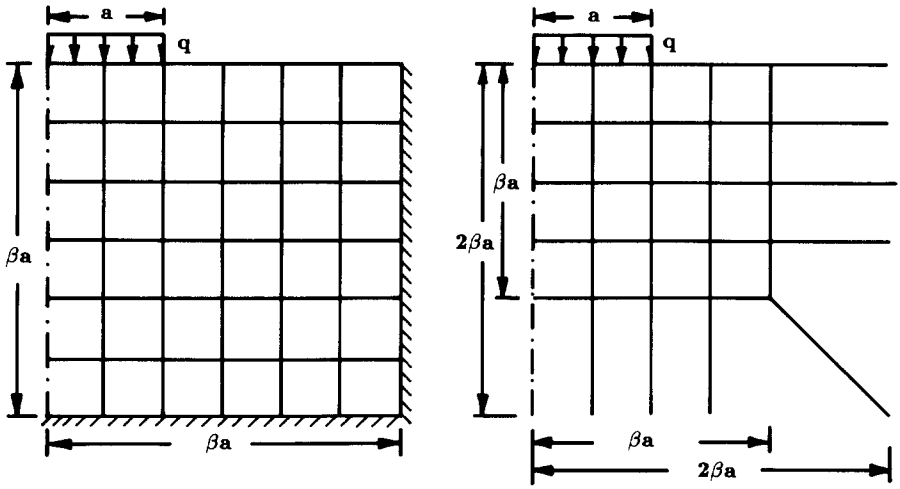


a) Conventional analysis

b) Coupled analysis

FIGURE 2. Typical meshes for analysis of surface footings

TABLE 1

Mapping and Shape Functions for 2-Dimensional Mapped Infinite Element

| Node | Mapping Functions | Shape Functions |
|---|---|---|
| 1 | $M_1 = \left(\frac{-2\xi}{1-\xi}\right)\left(\frac{\eta(1+\eta)}{2}\right)$ | $N_1 = \frac{1}{4}(1-\xi)(1+\eta) - \frac{1}{4}(1-\xi^2)(1+\eta) - \frac{1}{4}(1-\xi)(1-\eta^2)$ |
| 2 | $M_2 = \left(\frac{-2\xi}{1-\xi}\right)\left(\frac{-\eta(1-\eta)}{2}\right)$ | $N_2 = \frac{1}{4}(1-\xi)(1-\eta) - \frac{1}{4}(1-\xi)(1-\eta^2) - \frac{1}{4}(1-\xi^2)(1-\eta)$ |
| 3 | $M_3 = \frac{-2\xi}{(1-\xi)}(1-\eta^2)$ | $N_3 = \frac{(1-\xi)}{2}(1-\eta^2)$ |
| 4 | $M_4 = \frac{(1+\xi)}{(1-\xi)}\frac{(1-\eta)}{2}$ | $N_4 = (1-\xi^2)\frac{(1-\eta)}{2}$ |
| 5 | $M_5 = \frac{(1+\xi)}{(1-\xi)}\frac{(1+\eta)}{2}$ | $N_5 = (1-\xi^2)\frac{(1+\eta)}{2}$ |

values of $\beta$. Aspect ratios of individual elements for meshes in both methods are made approximately equal so that they would have the same errors due to mesh discretization.

When the boundary is truncated, nodal points on the boundary can be subjected to different boundary conditions (e.g. they can be fixed or permitted to move in the tangential direction to the boundary). It was observed that both boundary conditions yield the same results if the boundary is located at a reasonable distance. Consequently, all the nodes on truncated boundaries are fixed in the current study. In the coupled method, there is no truncated boundary and hence the nodes corresponding to infinite elements are left free. Conventional and coupled numerical solutions have been compared with the analytical solutions assuming linear elastic conditions in order to examine numerical solution accuracy and convergence as a function of boundary location. The soil is taken as a linear elastic, homogeneous, isotropic medium with Poisson's ratio of 0.2.

Flexible Circular Footing

This section considers the problem of the settlement and stress distribution below a flexible circular footing resting on the surface of a semi-infinite medium.

Typical finite element meshes are shown in Figure 2. The remoteness factor $\beta$ is defined in terms of the radius of footing $a$ and has been varied between tests (Table 2). In Table 2, NUMEL refers to the number of elements in the mesh and NDOF refers to the number of equations. The accuracy of the conventional and coupled numerical solutions can be expressed as a percentage of the settlement at the footing centre determined from analytical solutions [e.g. 8] as shown in Figure 3.

TABLE 2

Flexible Circular Footing Analyses

| Remoteness factor, $\beta$ | NUMEL/NDOF |
|---|---|
| Conventional Methods | |
| 2 | 25/150 |
| 5 | 25/150 |
| 10 | 49/294 |
| 20 | 49/294 |
| 40 | 81/490 |
| | |
| Coupled Methods | |
| 1.5 | 24/138 |
| 2 | 24/138 |
| 3 | 24/138 |
| 5 | 48/278 |

Figure 3 shows that when the infinite elements are located at a distance of 1.5 times the radius or greater, the percentage error in central displacement is less than 2%. However, in the conventional methods, the mesh has to be extended to about 20 times the footing radius to obtain solutions with less than 5% error. Significant errors in the conventional finite element analyses were observed for remoteness factors less than (say) 10. Figure 4 shows typical surface settlement profiles from analytical and numerical methods and illustrates that the coupled solution for $\beta = 2$ is more accurate than the conventional solution with $\beta = 10$. Table 2 shows that the coupled method with $\beta = 2$ uses 138 NDOF which is less than one half of the 294 NDOF used in the conventional analysis with $\beta = 10$. Since the computational effort is proportional to the square of NDOF the coupled method is about 4 times more efficient than the conventional method while achieving greater accuracy.

The results of numerical analyses for the same cases illustrated in Figure 4 showed that the predicted stress distributions are in close agreement with the analytical solutions. This observation can be anticipated based on the geometrical similarity between settlement profiles shown in Figure 4.

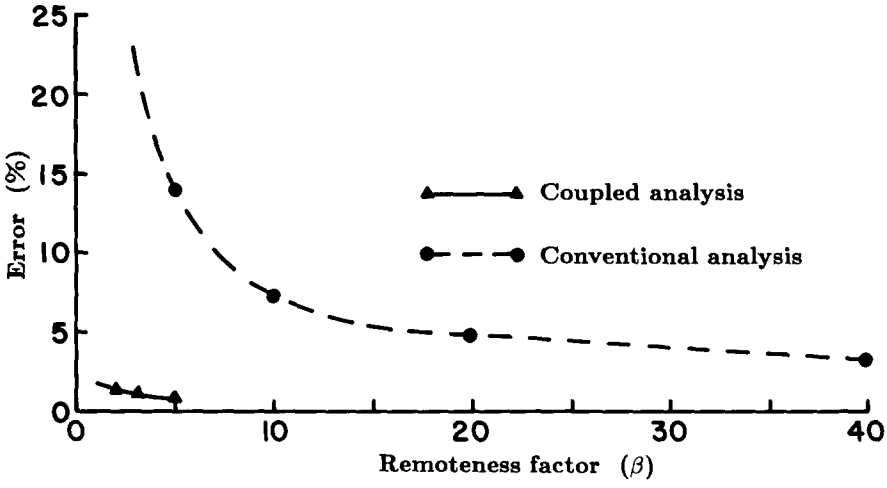


FIGURE 3. Variation of error in the central settlement of flexible circular footing

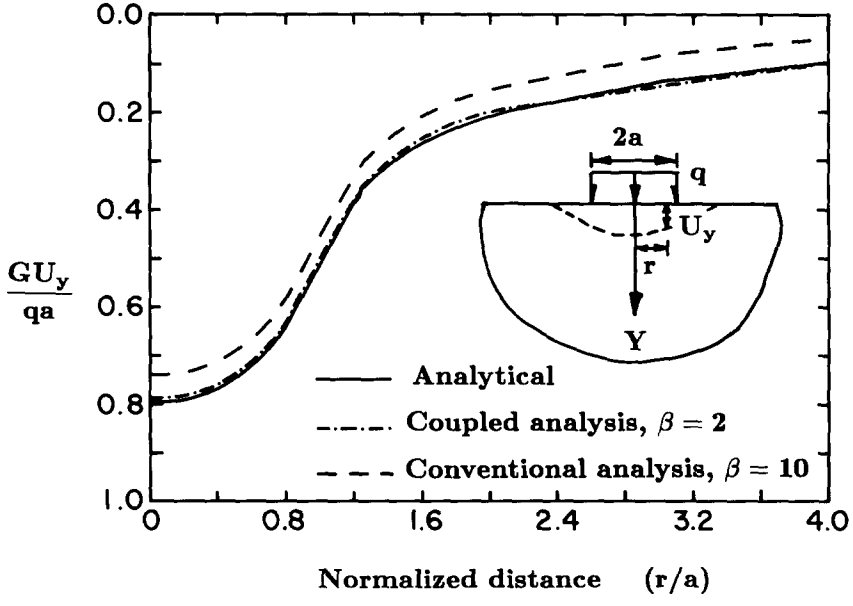


FIGURE 4. Surface settlement profile due to uniform loading from circular footing

Flexible Strip Footing

This section considers the problem of the settlement and stress distribution below a flexible strip footing resting on a semi-infinite medium. The same FEM meshes used for the circular footing case shown in Figure 2 are used in this section. The remoteness factor $\beta$ has been defined in terms of the footing half-width $B$. Analytical solutions for this case can be found in many text books [e.g. 9]. The surface settlement in analytical solutions is expressed as a function of an indeterminate parameter $d$, which is the distance to a plane parallel to the surface whose vertical displacement is zero. Parameter $d$ is usually taken as a large but finite value. As its value is unknown, predicted FEM values cannot be verified by any direct approach. However, an indication of the extent of infinite media that each FEM mesh represents can be obtained by back-calculating a $d$ value which gives the same analytical displacement profile as that predicted by FEM methods.

TABLE 3

Flexible Strip Footing Analyses

| Remoteness Factor, $\beta$ | NUMEL/NDOF | Predicted $d/B$ ratio |
|---|---|---|
| Conventional Methods | | |
| 10 | 49/294 | 12 |
| 20 | 49/294 | 23 |
| 40 | 81/490 | 44 |
| Coupled Methods | | |
| 2 | 24/138 | 41 |
| 5 | 48/278 | 103 |
| 10 | 48/278 | 205 |

Figure 5 shows typical normalized surface settlement profiles predicted by the numerical and analytical methods. Figure 5 and Table 3 show that the conventional methods can only model a domain corresponding to the mesh dimensions (i.e. $d/B \approx \beta$). In contrast, the coupled analyses are capable of modelling a region that extends well beyond the coupling boundary (i.e. $d/B >> \beta$).

Figure 6 shows the normalized stress distribution below the edge of a strip footing. The stresses for the coupled method were obtained with $\beta = 2$ and those for the conventional method using $\beta = 10$. The results indicate that the distribution of $\sigma_z$ is sensitive to the numerical method and the value of $\beta$ adopted. In addition, it was observed during

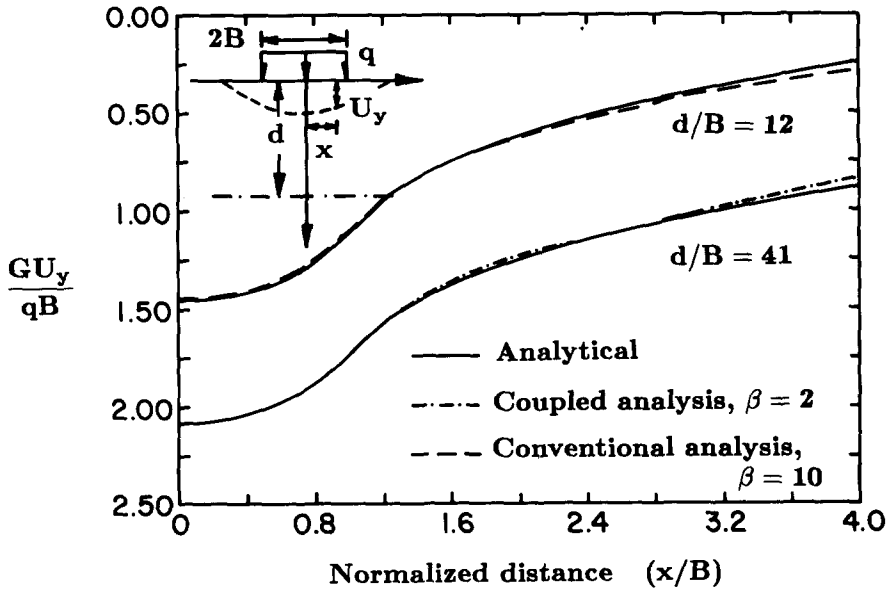


FIGURE 5. Surface settlement profile due to uniform loading from strip footing

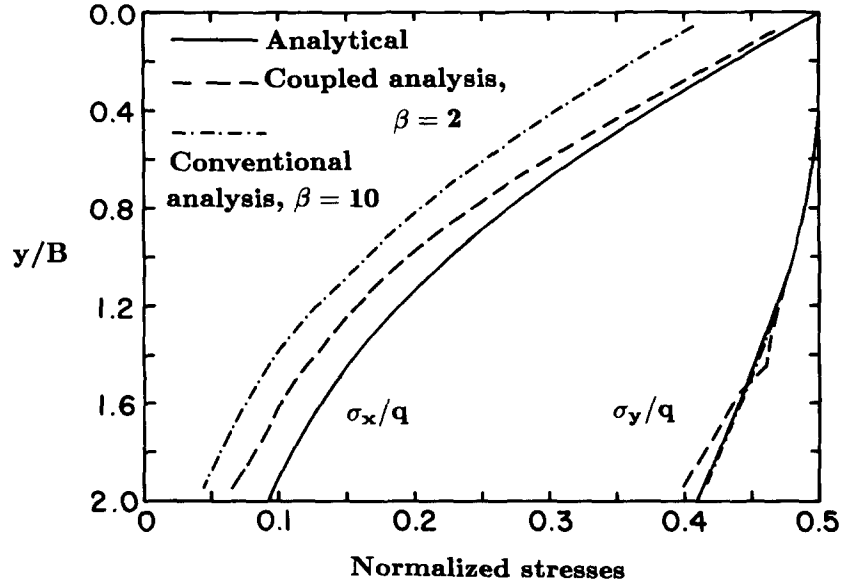


FIGURE 6. Stress distribution below edge of uniformly loaded flexible strip footing

the investigation that placement of the coupled boundary close to the footing does not introduce significant errors in predicted stress distributions.

Single Circular Pile

This section considers the problem of the settlement of an axially loaded circular pile which is perfectly bonded to the soil. Poulos and Davis [10,11] have reported extensive numerical solutions for the behaviour of piles of different slenderness ratios placed in media with a range of elastic properties. Their solutions are derived from finite difference analysis in conjunction with Mindlin's solution for displacements due to concentrated loads.

Numerical studies have been carried out with different values of $\beta$. The remoteness factor has been defined in terms of the length of pile $\ell$ as shown in Figure 7. Table 4 summarizes the mesh configurations investigated. It was observed that for very short piles, the solutions approach that of a circular footing. For very long piles both conventional and coupled numerical solutions converge since most of the load is transferred to the soil within the pile length.

TABLE 4

Circular Pile Analyses

| Remoteness factor, $\beta$ | NUMEL/NDOF |
|---|---|
| Conventional Methods | |
| 5 | 81/504 |
| 10 | 100/598 |
| 20 | 144/860 |
| | |
| Coupled Methods | |
| 0.5 | 48/296 |
| 1 | 63/384 |
| 5 | 99/596 |

Figure 8 shows the variation in percentage error with $\beta$ for intermediate slenderness ratios 5 and 25. For these slenderness ratios, coupled methods converge to less than 1% error at a $\beta$ value of 5 whereas the conventional methods require a value in excess of $\beta = 20$ to achieve the same degree of accuracy.

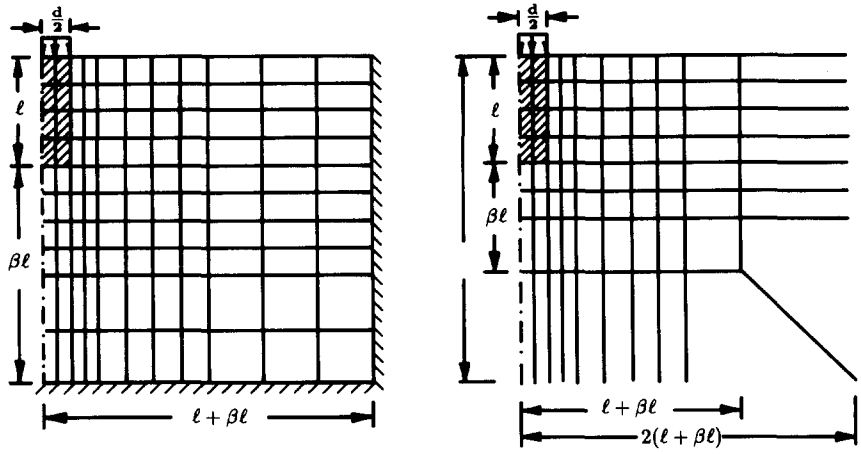


a) Conventional analysis

b) Coupled analysis

FIGURE 7. Typical meshes for axially loaded pile analysis

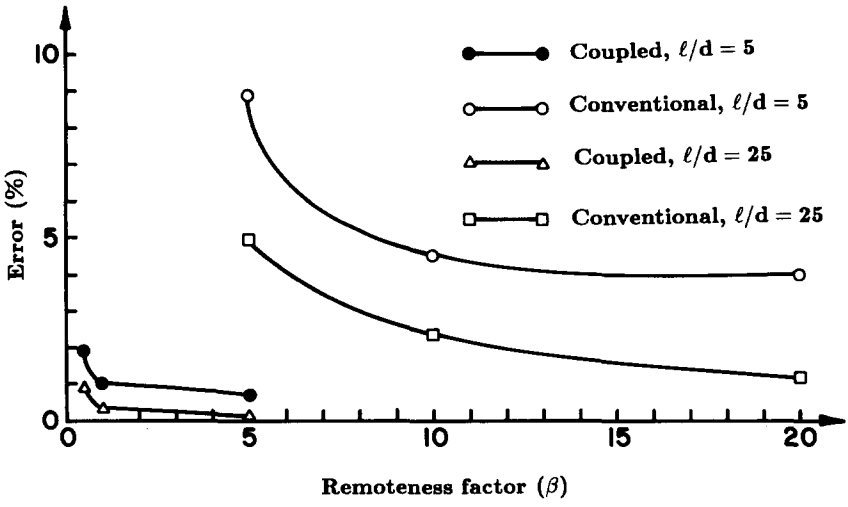


FIGURE 8. Variation of error in the settlement of axially loaded pile

Tunnel Excavated in a Prestressed Medium

When a tunnel is excavated in a prestressed elastic medium, radial and normal stresses are relieved which results in deformations around the tunnel periphery. Pender [12] has reported analytical solutions for the displacements caused by stress relief. Maximum radial displacement, $U_{max}$ occurs at the crown (i.e. $\theta = +90°$) and the minimum radial displacement, $U_{min}$ occurs along the horizontal axis (i.e. $\theta = 0°$). Using Poisson's ratio, $\nu = 0.2$ and lateral pressure coefficient $K_o = \nu/(1-\nu) = 0.25$, the displacements at these two locations simplify to:

$$U_{max} = 1.74\frac{\sigma_v}{E}a \tag{6}$$

$$U_{min} = -0.24\frac{\sigma_v}{E}a \tag{7}$$

Typical finite element meshes for numerical analyses are shown in Figure 9. The remoteness factor $\beta$ has been defined in terms of the radius of tunnel $a$. Relieved stresses are calculated at various $\theta$ values corresponding to the nodal point locations and they are applied as a non-uniform pressure loading on the tunnel periphery. Table 5 summarizes the various cases analyzed.

TABLE 5

Tunnel Analyses

| Remoteness factor, $\beta$ | NUMEL/NDOF |
|---|---|
| Conventional Methods | |
| 2 | 9/64 |
| 3 | 15/102 |
| 4 | 15/102 |
| 5 | 15/102 |
| 10 | 18/120 |
| 20 | 18/120 |
| 40 | 21/138 |
| | |
| Coupled Methods | |
| 1 | 3/18 |
| 1.5 | 9/54 |
| 2 | 12/72 |

Figures 10 and 11 show the variation of percentage error in maximum and minimum displacements with remoteness factor $\beta$. It can be seen that the coupled methods converge

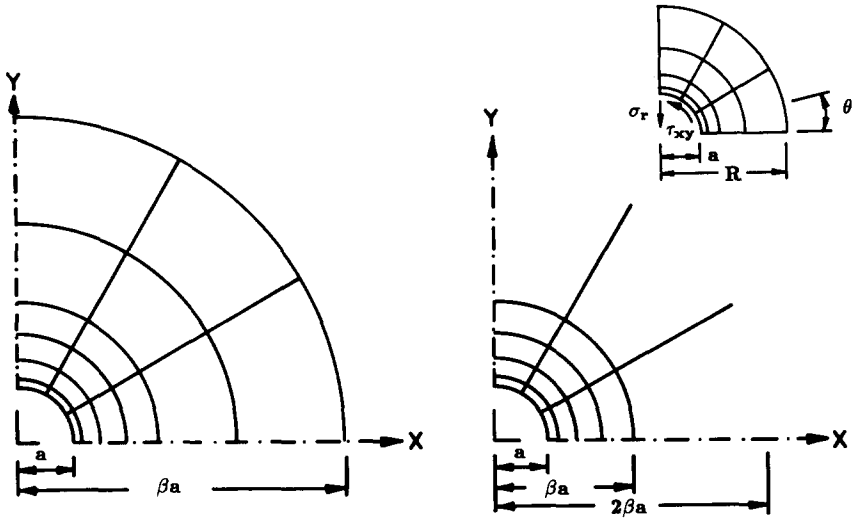


a) Conventional analysis

b) Coupled analysis

FIGURE 9. Typical meshes for tunnel analysis

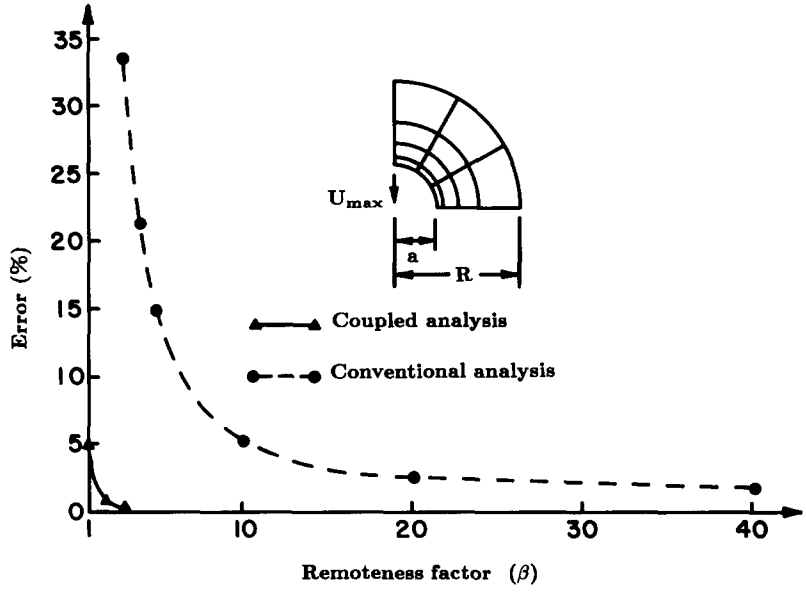


FIGURE 10. Variation of error in $U_{max}$

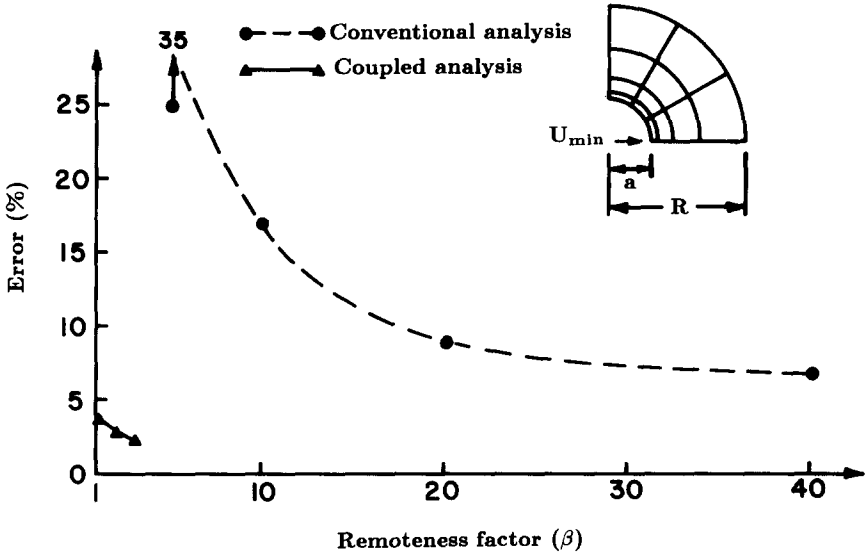


FIGURE 11. Variation of error in $U_{min}$

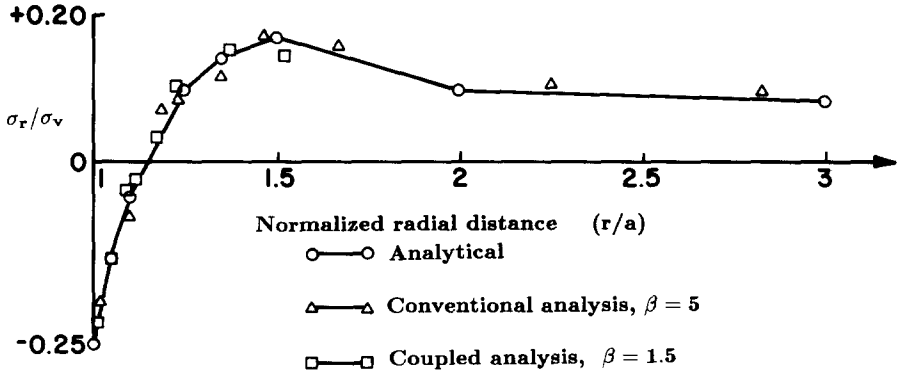


FIGURE 12. Radial stress distribution along $\theta = 0°$ radial line

to the analytical values rapidly (i.e. less than 0.5% at $\beta = 2$) whereas the conventional methods show errors of about 2 to 6% for a large number of elements with the mesh boundary located at 40 times the radius. Figure 12 shows the analytical and predicted incremental radial stresses along the $\theta = 0$ radial line. Stresses for the coupled methods were obtained by placing infinite elements at 1.5 times the radius and the boundary for conventional analysis at 5 times the radius. Both methods predict stress distributions reasonably well.

## CONCLUSIONS

Numerical solutions representing four classical geomechanics problems have been obtained using conventional finite elements and finite elements coupled to infinite elements to represent a semi-infinite elastic medium. Solutions obtained by both methods were compared with analytical values and the errors due to the proximity of the truncated boundary in conventional methods compared to the errors due to proximity of the coupled boundary using infinite elements. It was observed that the location of the truncated boundary can introduce significant errors in predicted settlements and stresses using conventional finite element methods even when the truncated boundary is located at more than 10 times the characteristic length of the structure. In contrast, numerical solutions using coupled methods were seen to converge to analytical solutions very rapidly with respect to number of elements while requiring significantly fewer degrees of freedom. The results of this study show that a high degree of accuracy can be obtained using infinite elements coupled with finite elements at a distance of twice the radius or half-width of footings or tunnels and about 5 times the pile length for piles with intermediate slenderness ratio values.

Combination of $1/r$ type mapped infinite elements with a lower order of integration than that for regular finite elements in the assemblage is recommended for best efficiency.

The computational accuracy and efficiency of coupled methods for the solution of plasticity problems in geomechanics is currently under study by the authors.

## REFERENCES

1. Bettess, P., Infinite element. Int. J. Num. Meth. Eng. 11 (1977) 53-64.
2. Curnier, A., A static infinite element. Int. J. Num. Meth. Eng. 19 (1983) 1479-1488.
3. Beer, G. and Meek, J.L., Infinite domain elements. Int. J. Num. Meth. Eng. 17 (1981) 43-52.
4. Zienkiewicz, O.C., Emson, C. and Bettess, P., A novel boundary infinite element. Int. J. Num. Meth. Eng. 19 (1983) 393-404.
5. Kumar, P., Static infinite element formulation. J. Struct. Div., A.S.C.E. 111 (1984)

2355-2372.

6. Marques, J.M.C. and Owen, D.R.J., Infinite elements in quasi-static materially non-linear problems. Comp. and Struct. 18 (1984) 739-751.
7. Selvadurai, A.P.S. and Gopal, K.R., Consolidation analysis of screw plate test. Proc. 39th Canadian Geotech. Conf., Ottawa. (1986) 167-178.
8. Timoshenko, S. and Goodier, J.N., Theory of Elasticity. McGraw Hill Book Co. Inc., New York, N.Y. (1951).
9. Saada, A.S., Elasticity: theory and applications. Pergamon Press, New York, N.Y. (1974)
10. Poulos, H.G. and Davis, E.H., The settlement behaviour of single axially loaded piles and piers. Geotechnique 18. (1968) 351-371.
11. Poulos, H.G. and Davis, E.H., Elasticity Solutions for Soil and Rock Mechanics. J. Wiley and Sons, New York, N.Y. (1974).
12. Pender, M.J., Elastic solutions for a deep circular tunnel. Geotechnique 30. (1980) 216-222.

Received 15 March 1988; revised version received and accepted 26 July 1988